Journal of Fluids and Structures (2002) **16**(8), 1059–1071
doi:10.1006/jfls.2002.0469 available online at http://www.idealibrary.com on IDEAL®

FLOW PAST TWO CYLINDERS IN TANDEM: INSTANTANEOUS AND AVERAGED FLOW STRUCTURE

J.-C. Lin, Y. Yang[1] and D. Rockwell*

Department of Mechanical Engineering and Mechanics, 354 Packard Laboratory 19 Memorial Drive West, Lehigh University, Bethlehem, PA 18015-3085, USA

(Received 7 January 2001, and in final form 9 December 2001)

A technique of high-image-density particle image velocimetry is employed to characterize the instantaneous and averaged patterns of velocity, vorticity and Reynolds stress due to flow past two cylinders in tandem. These features of the flow patterns are characterized in the gap region as a function of the distance between the cylinders. In turn, they are related to the patterns in the near-wake of the two-cylinder system. Along the gap between the cylinders, small-scale concentrations of vorticity are formed in the separated shear layers. These concentrations buffet the surface boundary layer on the downstream cylinder, and thereby influence the eventual shedding of large-scale vortices. Within the gap, the instantaneous structure of the recirculation zones can exhibit both symmetrical and asymmetrical patterns. In the near-wake of the downstream cylinder, the form of the vortex shedding, as well as the averaged patterns of the flow structure, are substantially altered, relative to the case of a single cylinder. The width of the near-wake, as represented by averaged patterns of vorticity, is substantially narrower and the magnitudes of the peak Reynolds stress are significantly attenuated. On the other hand, if the gap region is sufficiently large such that Kármán-like vortices form between the cylinders, the near-wake of the downstream cylinder shows distinctive patterns, and both the wake width and the magnitude of the Reynolds stresses become larger, relative to those at smaller gap width.

1. INTRODUCTION

Flow past two cylinders in tandem, whereby one cylinder is located downstream of the other, represents an important and remarkably complex flow configuration. In essence, the wake from the downstream cylinder is a strong function of both the steady and unsteady vorticity field incident upon it. The nature of this vorticity field is, of course, directly related to the gap between the tandem cylinders. From an experimental standpoint, the primary emphasis has been on determination of the time-averaged forces and surface pressures, most notably the base pressure, occasionally in conjunction with qualitative flow visualization. Using these approaches, it has been possible to gain insight into the cylinder loading and the overall flow characteristics. Zdravkovich (1977, 1982, 1987) provided an overview of loading characteristics and flow patterns. Zdravkovich & Pridden (1977) emphasized the discontinuous jump in base pressure at a critical spacing of the cylinders $L/D = 3{\cdot}5$, in which L is the distance between centers of the cylinders and D

[1] On leave from Beijing Institute of Aerodynamics (BIA).

*Corresponding author. Tel.: +1-610-758-4107; fax: +1-610-758-4041

0889-9746/02/081059 + 13 $35.00/0

is the cylinder diameter. Classifications of the qualitative flow regimes of the tandem cylinder arrangement are provided by Igarashi (1981, 1984) and Zdravkovich (1982). In essence, below a threshold value of L/D, referred to in the literature as the critical spacing, no vortex shedding occurs in the gap region between the cylinders, whereas above it, vortex shedding occurs from both cylinders. This threshold appears to be a function of Reynolds number. Qualitative flow visualization of the gap and near-wake region of the two-cylinder system is provided by Ishigai *et al.* (1972), Ljungkrona *et al.* (1991), Ljungkrona & Sundén (1993), and Wu *et al.* (1994). Ljungkrona *et al.* (1991, 1993) clearly show the important influence of Reynolds number. Furthermore, Ljungkrona *et al.* (1991) addressed the influence of the free-stream turbulence, and found that the critical spacing of the cylinders decreased as turbulence intensity increased. Ishigai *et al.* (1972) showed qualitative portraits of change in the gap and near-wake flow patterns as the gap spacing was varied. Wu *et al.* (1994) show hydrogen bubble images of both the quasi-two-dimensional and spanwise patterns of the flow structure and, furthermore, provide spanwise coherence distributions (via hot-wire measurements) as a function of gap width.

Igarashi (1981, 1984) considered a wide parameter range of Reynolds number versus gap spacing and defined a number of flow regimes in addition to those described in the foregoing. Unstable and bistable states, as well as jumps between states, are representative of the complex phenomena that can occur in a tandem cylinder arrangement.

Distributions of root-mean-square (r.m.s.) pressure about the surface of the downstream cylinder have been measured by Arie *et al.* (1983), Igarashi (1984), Ljungkrona *et al.* (1991) and Ljungkrona & Sundén (1993). The common feature of all of these distributions of fluctuating pressure is the occurrence of a well-defined peak(s) on the forebody region of the downstream cylinder at smaller values of cylinder gap, presumably a result of the unsteadiness of the impinging shear layer. At larger values of gap spacing L/D, these peaks can become particularly large, perhaps due to the impingement of Kármán-like vortices formed in the gap region.

Other types of characterizations of the gap region have involved surface oil-flow patterns, fluctuating pressure, surface film sensor, and surface heat transfer measurements. Igarashi (1984) employed surface oil patterns to show the relationship between the reattachment line and the pressure distribution on the downstream cylinder. Arie et al. (1983) also determined the root-mean-square lift and drag on the downstream cylinder, which exhibited much larger values than on the upstream cylinder. Lee *et al.* (1997) employed surface-mounted hot film sensors to provide simultaneous records of fluctuations about the periphery of the cylinder; a number of harmonics were evident in the unsteady signals in the base region. Hiwada *et al.* (1982) pursued the relation between local heat transfer and fluctuation velocity (via a hot-wire probe), and found that the overall Nusselt number was 20–30% higher than for a single cylinder.

Numerical simulation of the vortex patterns and steady and unsteady loading at low Reynolds number was undertaken by Stansby *et al.* (1987) and Slaouti & Stansby (1992) using a vortex method. Recent efforts, employing different types of numerical simulation, include those of Mittal *et al.* (1997) and Farrant *et al.* (2000), also at relatively low values of Reynolds number.

In the event that one or both cylinders in a tandem arrangement are elastically mounted, the mechanisms giving rise to self-excited oscillations are particularly challenging. Chen (1985) addressed the overall response characteristics of the cylinder system and defined mechanisms of the fluid–elastic instability. Zdravkovich (1985) focused on the manner in which the instability of the two-cylinder system arose and classified the nature of the fluid–elastic response. King & Johns (1976) showed that oscillations in both the cross-flow and in-flow directions may occur. Mahir & Rockwell (1996) subjected two tandem cylinders to

controlled oscillation, with a prescribed phase angle between them and classified the modulated and locked-on response of the near-wake, in conjunction with the spectra of the wake velocity fluctuations. When considering elastic oscillations of the tandem cylinder system, it is important to distinguish between vibrations associated with vortex shedding and those due to a mechanism of interference galloping. Knisely & Nakagawa (1988), Knisely & Kawagoe (1990), and Knisely *et al.* (1995) addressed a central feature, namely the phase lag, or delay time, between the cylinder motion and the unsteady lift force acting on the downstream cylinder that underwent oscillations.

The tandem cylinder arrangement may be viewed as an idealization of an array of a large number of cylinders and, no doubt, certain of the features generic to the tandem configuration may be present, at least to a degree, in an array. Païdoussis (1982), Chen (1984, 1987), Païdoussis & Price (1988) and Weaver & Fitzpatrick (1988) determined design guidelines and undertook quasi-analytical descriptions of this intriguing class of cylinder systems. Hetz *et al.* (1991) focused on the special configuration of five in-line cylinders and observed alternate vortex shedding in the gaps for a range of gap spacing. Ziada & Oengören (1993) defined regimes of vortex shedding involving either coupled or uncoupled interaction between adjacent wakes in an entire array. Price & Serdula (1995) used qualitative visualization to characterize the vortex shedding in an array of risers. Most recently, Sumner *et al.* (2000) employed a technique of particle image velocimetry to classify the flow patterns occurring in staggered configurations of two cylinders. Important features include shear layer reattachment, induced separation, vortex pairing and synchronization and vortex impingement.

The foregoing investigations have provided important insight into various features of the tandem cylinder system. Relatively little is understood, however, of the detailed flow structure, in both an instantaneous and time-averaged sense. In particular, for the range of higher Reynolds numbers of interest in the present investigation, where small-scale Kelvin–Helmholtz instabilities form in the separated shear layers, their existence is expected to alter substantially the patterns of instantaneous vorticity and averaged Reynolds stress in the gap region, as well as in the near-wake of the cylinder system. Such features are evident for the case of a single cylinder, as shown by Chyu & Rockwell (1996). Moreover, within the gap region between the two cylinders, the possibility of instantaneous and averaged asymmetries of the flow patterns, and their consequence on the near-wake of the downstream cylinder, is of interest. All of these features are expected to be a function of the magnitude of the gap between the cylinders.

Regarding the near-wake of the downstream cylinder, the nature of possible formation of Kármán-like vortices, in relation to those formed from a single cylinder, is unclarified. Furthermore, the relationship between averaged patterns of vorticity, Reynolds stress and streamline topology has not been addressed. The aim of this investigation is to address these issues using a technique of quantitative imaging.

2. EXPERIMENTAL SYSTEM AND TECHNIQUES

An overview of the two-cylinder system is shown in Fig. 1(a). Each cylinder had a diameter $D = 50{\cdot}8$ mm and a length $L_c = 420$ mm. The two-cylinder system was supported by false walls. The leading edge of the false wall, which was beveled to a sharp edge along its exterior surface, extended a distance of 50·8 mm upstream of the center-line of the upstream cylinder. Moreover, the trailing edge of each wall extended a distance 356 mm downstream of the center-line of the upstream cylinder. The height of each false wall was 660 mm. The magnitude of the spacing L between the cylinders could be adjusted by

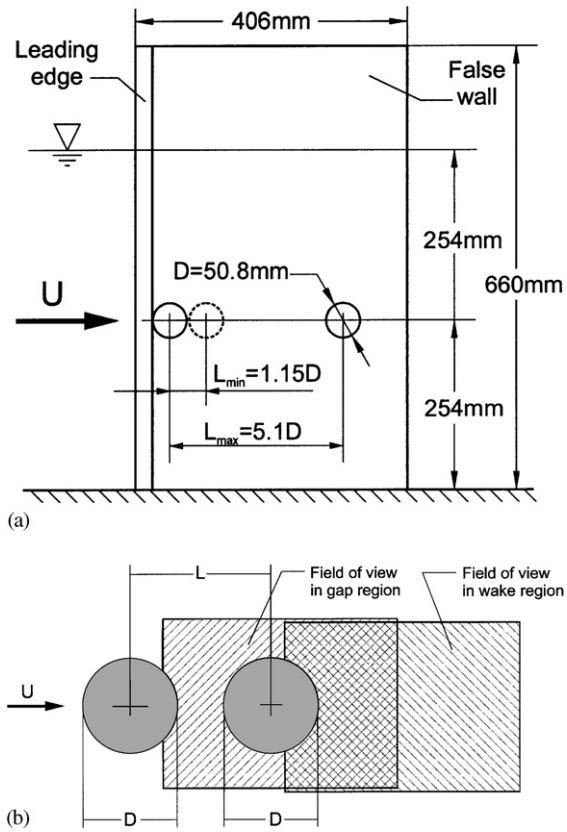

Figure 1. (a) Schematic of the two-cylinder system mounted between false walls. (b) Schematic of two cylinders in tandem showing two principal fields of view for quantitative imaging. The first field of view concentrates on the gap region and the second on the near-wake region.

translating the downstream cylinder, while the upstream cylinder remained fixed. The entire cylinder/end-plate system was suspended in the test-section of the large-scale water channel, which had a width of 927 mm, a depth of 610 mm and a length of 4880 mm. The water height was maintained at an elevation of 508 mm. Throughout the experiments, an inflow velocity $U = 192$ mm/s was employed, yielding a Reynolds number, based on cylinder diameter, of $\mathrm{Re} = 10\,000$.

A digital technique of high-image-density particle image velocimetry was employed to determine the quantitative flow patterns generated by the two-cylinder system. A dual-pulsed Yag laser system was employed to generate a laser sheet. The output of the laser was transmitted through a cylindrical lens, which generated the planar laser sheet located at a distance of 55 mm from the interior of the false wall. This laser sheet illuminated small particles with a diameter of 12 μm, which were seeded in the flow. The particles were metallic coated, hollow plastic spheres. Images were recorded using a digital camera having a resolution of 999×960 pixels. A frame-to-frame correlation technique was employed to determine the velocity vector for each interrogation area. The dimensions of the interrogation area employed throughout were 32×32 pixels square, and an overlap of 50% was employed. The high-image-density criterion was satisfied by ensuring that a minimum of 50 particle images was contained within the interrogation area. The effective grid size in the plane of the laser sheet was 2·1 mm, yielding a total of approximately 3720 velocity vectors. For the images shown herein, regions of the freestream above and below

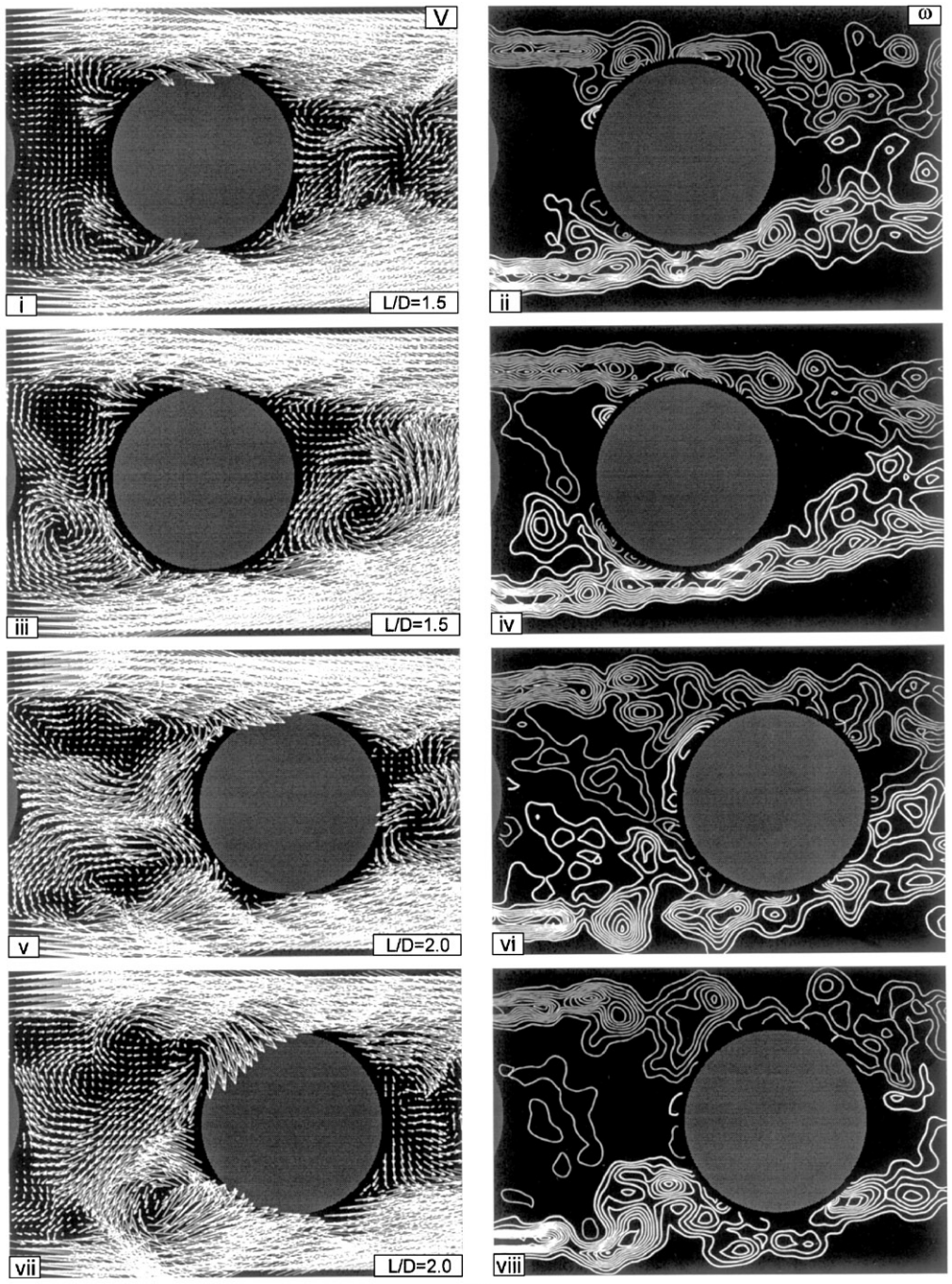

(a)

Figure 2. (a) Comparison of instantaneous states of the flow at a cylinder spacing L normalized with respect to cylinder diameter D of $L/D = 1{\cdot}5$ and $2{\cdot}0$. For vorticity patterns, minimum $\omega_{\min}$ and incremental $\Delta\omega$ are both $5\,s^{-1}$. (b) Instantaneous states of the flow at a large cylinder spacing L, normalized with respect to the cylinder diameter D, of $L/D = 5.1$ (top row of images). For patterns of vorticity, the minimum $\omega_{\min}$ and incremental $\Delta\omega$ are both $5\,s^{-1}$. The image at the lower right is from Gaydon and Rockwell (1999).

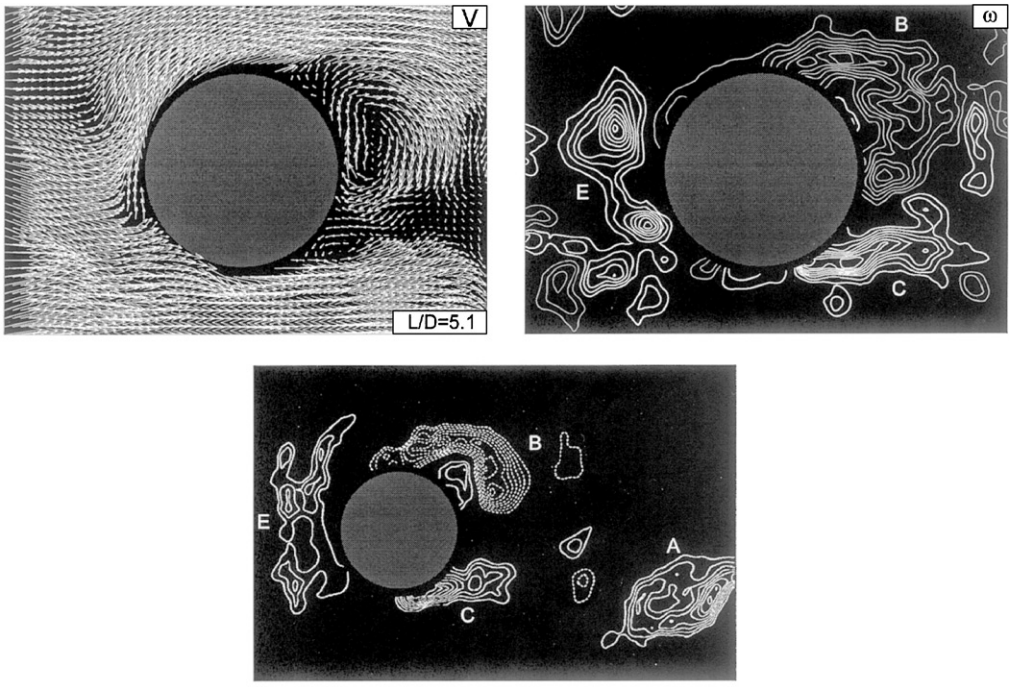

(b)

Figure 2. *(Continued)*

the two-cylinder system, which are not of interest, have been cropped, in order to yield the fields of view shown in Fig. 1(b).

Images of instantaneous velocity fields were employed to attain instantaneous vorticity. In addition, an average of 50 instantaneous images led to averaged values of velocity $\langle V \rangle$, vorticity $\langle \omega \rangle$, normalized Reynolds stress $\langle uv \rangle / U^2$, and averaged streamline topology. In addition, phase-averaged representations of the flow were employed to provide a guide for interpretation of instantaneous images. Four instantaneous images were employed for each average.

3. FLOW PATTERNS IN GAP REGION

Figs. 2 and 3 focus on the major features of the flow patterns in the gap region as a function of dimensionless cylinder spacing L/D. A number of images show both the gap and the near-wake region; the latter will be considered in a subsequent section.

Fig. 2(a) shows instantaneous patterns of velocity and vorticity for two values of dimensionless cylinder spacing $L/D = 1{\cdot}5$ and $2{\cdot}0$. For each value of L/D, two instantaneous images are shown. They represent the basic types of instantaneous states, which involve symmetrical and asymmetrical patterns in the gap region. Velocity image (i) corresponds to the case $L/D = 1{\cdot}5$. It exhibits a symmetrical pattern of jet-like flows from its upstream surface. As shown in the corresponding vorticity image (ii), these jet-like regions are associated with adjacent positive and negative contours of vorticity along the upstream surface of the cylinder. Small, low-level concentrations of vorticity are identifiable in the shear layers along the upper and lower sides of the gap. Moreover, the velocity image (iii) for the case $L/D = 1{\cdot}5$ shows two recirculation zones of different character within the gap. The recirculation in the lower portion of the gap exhibits a well-defined swirl pattern of velocity vectors, in contrast to that in the upper portion. As shown in the corresponding vorticity image (iv), the lower recirculation region is associated with a concentration of positive (thick white line) vorticity. On the other hand, in the upper portion of the gap, there is no significant concentration of vorticity. Again, as in image (ii), the shear layers along the upper and lower sides of the gap indicate definable, small-scale concentrations of vorticity.

The images of instantaneous velocity and vorticity in images (v)–(viii) of Fig. 2(a) correspond to $L/D = 2{\cdot}0$. It is evident that image (v) corresponds to a nearly symmetrical pattern of velocity. A jet flow of substantial magnitude, which is oriented in the upstream direction, exists along the center-line of the gap. Swirl patterns of velocity vectors occur on the lower and upper sides of this jet-like flow. The corresponding pattern of instantaneous vorticity of image (vi) shows that broadly distributed regions of vorticity exist in the recirculation zones on the upper and lower sides of the jet. In the separated shear layers bounding the upper and lower sides of the gap region, however, pronounced concentrations of vorticity are evident. In fact, the coalescence of adjacent concentrations occurs in the upper shear layer as it impinges upon the surface of the cylinder. Concerning images (vii) and (viii) at $L/D = 2{\cdot}0$, a particularly well-defined swirl pattern of velocity vectors occurs in the lower region of impingement upon the cylinder. This region is associated with a larger-scale cluster of vorticity. On the other hand, only a weakly defined pattern of swirl occurs at the location of impingement of the upper shear layer, and it is located further upstream of the surface of the cylinder.

Considering the images of Fig. 2(a) as a whole, it is evident that the instantaneous flow pattern exhibits intermittency between nearly symmetrical and asymmetrical patterns of velocity and vorticity.

Instantaneous patterns of velocity and vorticity are shown in Fig. 2(b) for the limiting case $L/D = 5{\cdot}1$. The gap between the cylinders is sufficiently large that Kármán-like vortices form in the gap region. Such a large-scale vortex is represented by the vertical, elongated cluster of positive vorticity E in the image at the top right of Fig. 2(b). The consequence of such incident vorticity is the rapid appearance of large-scale vortices in the wake of the cylinder, which are represented by the concentration of negative vorticity B from the upper side of the cylinder, and the positive layer of vorticity C from the lower side of the cylinder. This pattern of vortices E, B and C suggests a phase relationship between the arrival of a large-scale region of vorticity at the upstream face of the cylinder and the timing of vortices B and C shed in the near-wake. In fact, this phase relationship is the same as that observed in the related investigation of Gaydon and Rockwell (1999), in which both the upstream and downstream cylinder were subjected to controlled oscillation in the transverse direction. As is evident in the image of the lower right of Fig. 2(b), the relative scale and position of vortices E, B and C is generally similar to that in the image at the upper right.

Fig. 3 shows patterns of averaged velocity $\langle V \rangle$, vorticity $\langle \omega \rangle$, and Reynolds stress $\langle uv \rangle / U^2$. Consider, first of all, the velocity and vorticity images. For the cases $L/D = 1{\cdot}5$ and 2·0, swirl patterns of velocity vectors exist in the gap region. It is evident that these patterns are not symmetrical with respect to the center-line of the gap. That is, an asymmetrical bias is present, despite the geometrical symmetry. This is especially so at $L/D = 1{\cdot}5$, for which patterns of concentrated vorticity are evident in the lower region of the gap, but not in the upper region. On the other hand, the broadly distributed regions of vorticity for $L/D = 1{\cdot}5$ tend toward a symmetrical pattern. Comparison of the images at $L/D = 1{\cdot}15$, with those at $L/D = 1{\cdot}5$ and 2·0, shows that no well-defined swirl patterns, i.e., recirculation zones, are evident in the gap region. At the other extreme, corresponding to $L/D = 5{\cdot}1$, the cylinders are widely spaced and recirculation eddies do not exist in this case as well. Layers of positive and negative vorticity are confined to the region immediately adjacent to the upstream surface of the cylinder, and are associated with the unsteady impingement of the large-scale Kármán vortices upon the upstream surface of the cylinder. In contrast, for the case $L/D = 2{\cdot}0$, the distinctive patterns are associated with the quasi-stationary recirculation vortices occurring in the gap region. Patterns of Reynolds stress are shown in the right column of Fig. 3. They indicate that, as the cylinder spacing L/D increases, higher levels of Reynolds stress exist further upstream of the cylinder. At $L/D = 1{\cdot}15$, contours of Reynolds stress are barely detectable upstream of the center of the cylinder; at $L/D = 1{\cdot}5$, they are more clearly defined; and at $L/D = 2{\cdot}0$, substantial levels of Reynolds stress are evident at a distance of nearly one cylinder diameter upstream. This trend occurs in conjunction with the enhanced development of the small-scale vortical structures with increasing size of the gap, which is evident in the instantaneous images of Fig. 2(a). On the other hand, the Reynolds stress patterns for $L/D = 5{\cdot}1$ are completely different. Thick layers of high $\langle uv \rangle / U^2$ exist along the upstream face of the cylinder and, upstream of these layers, lower level regions of opposite-signed $\langle uv \rangle / U^2$ occur. This fundamentally different pattern of Reynolds stress is apparently due to the rapid distortion of the large-scale Kármán structures, which are formed in the gap region and impinge upon the leading surface of the cylinder.

4. FLOW PATTERNS IN THE NEAR-WAKE

Patterns of velocity and vorticity in the near-wake region are shown in Fig. 4. Images are illustrated for the reference case of a single cylinder, as well as cylinders having various

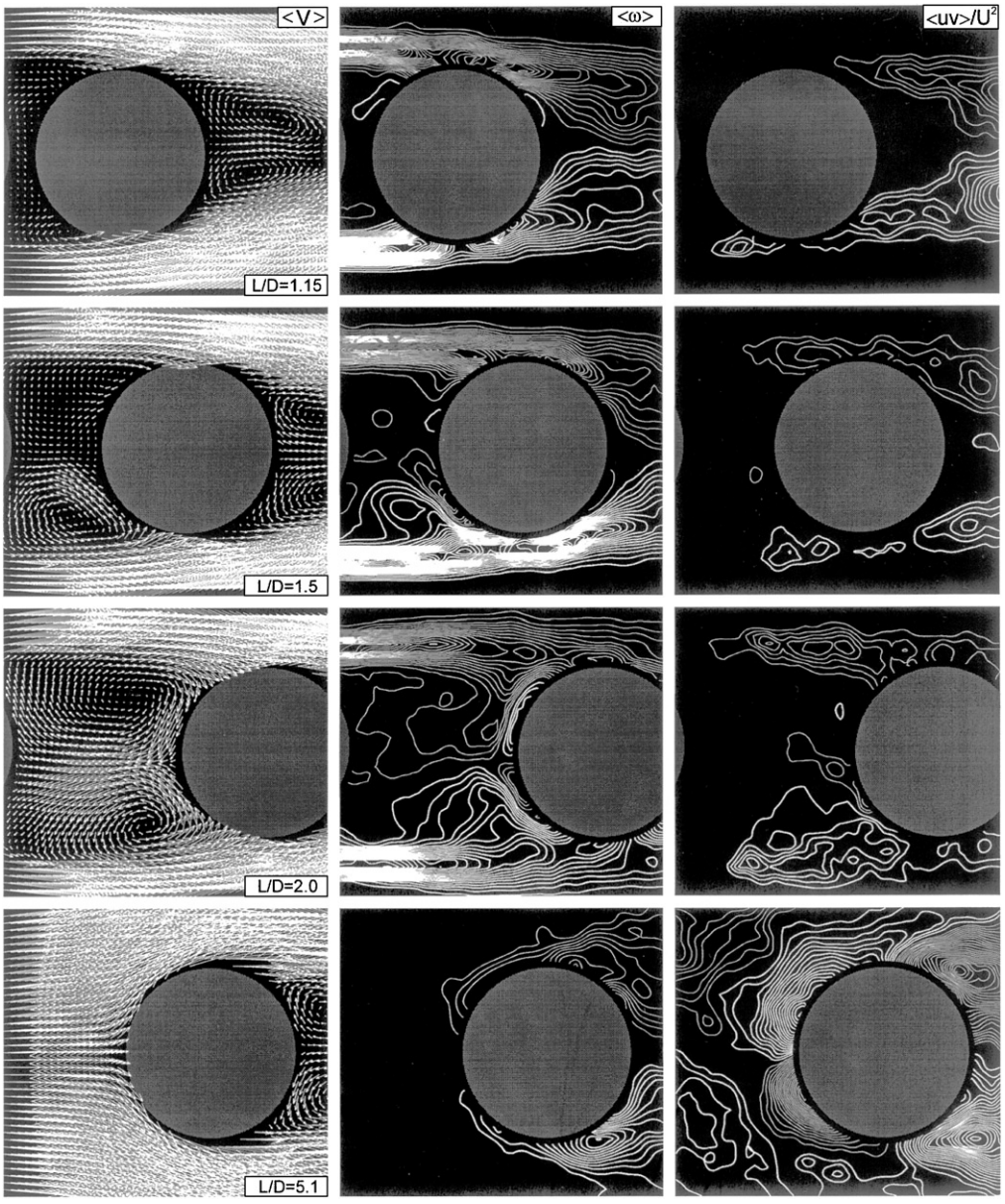

Figure 3. Averaged flow structure in gap and very near-wake region of downstream cylinder as a function of dimensionless cylinder spacing L/D. Patterns of averaged velocity $\langle V \rangle$, vorticity $\langle \omega \rangle$ and Reynolds stress $\langle uv \rangle / U^2$ are shown. For vorticity patterns, minimum $\langle \omega_{\min} \rangle$ and incremental $\langle \Delta\omega \rangle$ are both $2\,s^{-1}$. For contours of constant Reynolds stress normalized by the free-stream velocity, $\langle uv \rangle / U^2$, minimum and incremental levels are both 0·005.

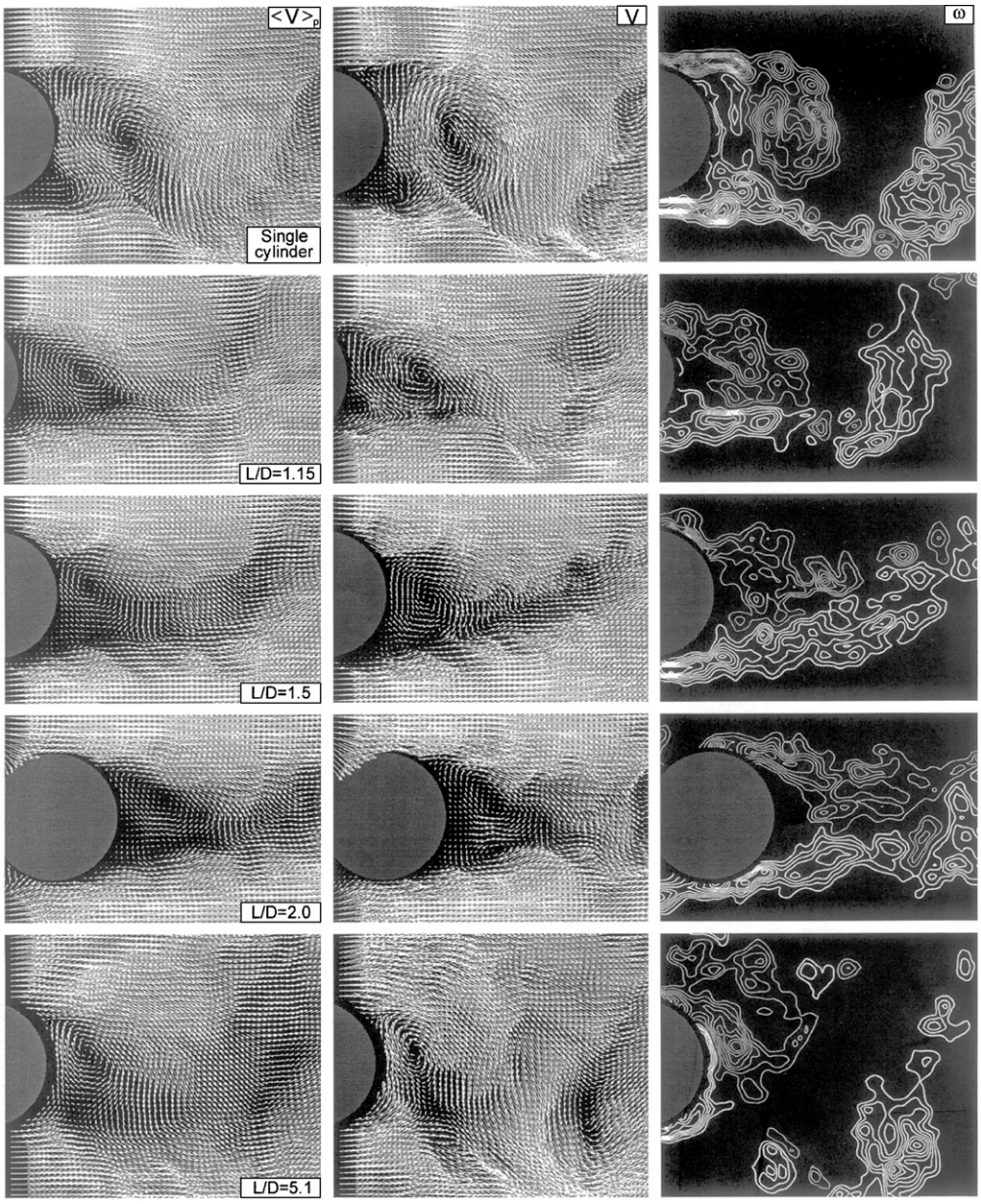

Figure 4. Images of phase-averaged $\langle V \rangle_p$ and instantaneous V velocity patterns in comparison with patterns of instantaneous vorticity ω at various values of dimensionless cylinder spacing L/D in comparison with the case of a single cylinder. For vorticity patterns, minimum $\omega_{\min}$ and incremental $\Delta\omega$ are both $5\,s^{-1}$.

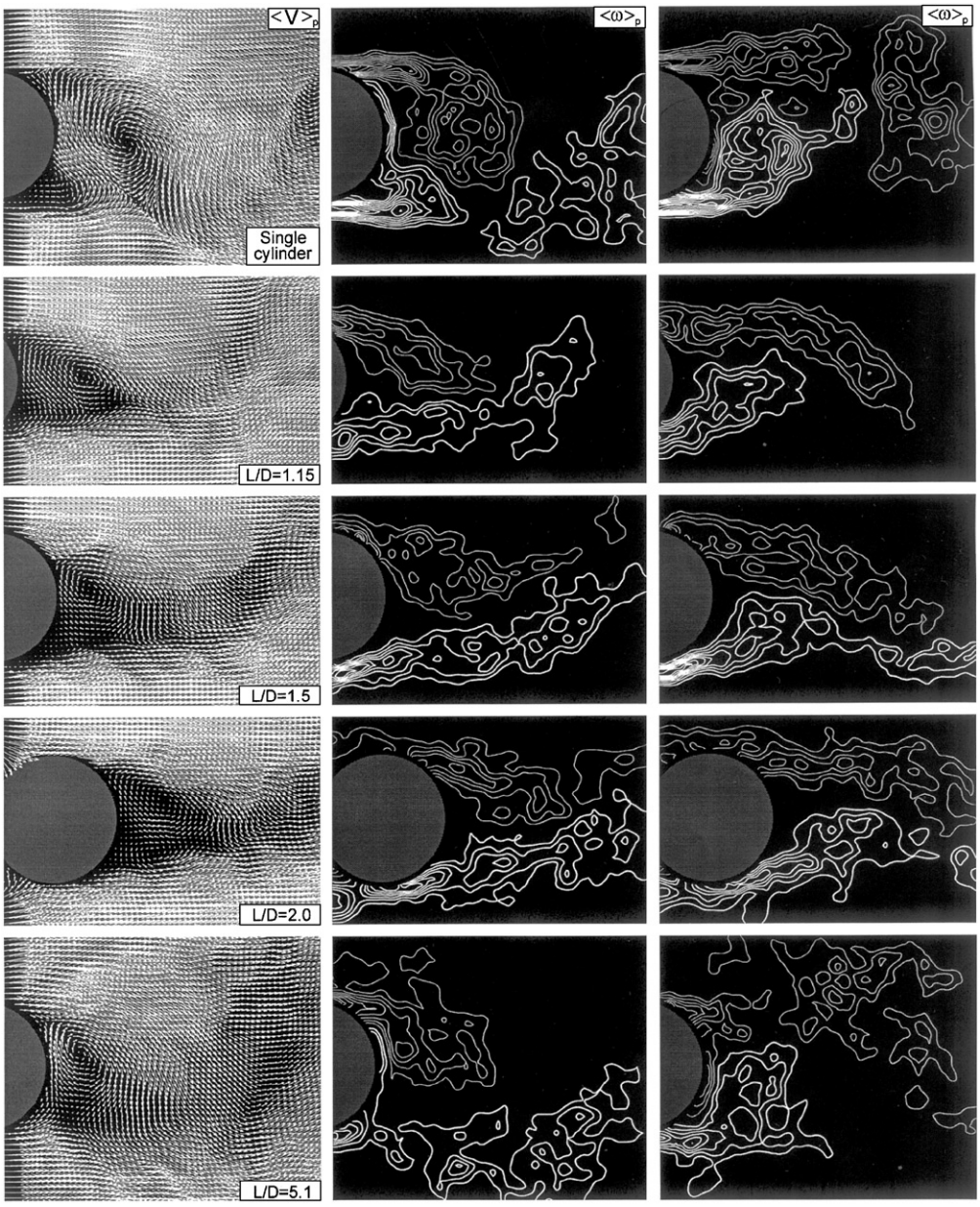

Figure 5. Phase-averaged patterns of velocity $\langle V \rangle_p$ and vorticity $\langle \omega \rangle_p$ as a function of dimensionless cylinder spacing L/D relative to the case of a single cylinder. The middle column of images shows phase-referenced case corresponding to formation of a large-scale vortex from the upper surface of the cylinder and right column of images for vortex formation from the lower surface of the cylinder. For vorticity patterns, minimum $\langle \omega_{\min} \rangle$ and incremental $\langle \Delta\omega \rangle$ are both $5\,\mathrm{s}^{-1}$.

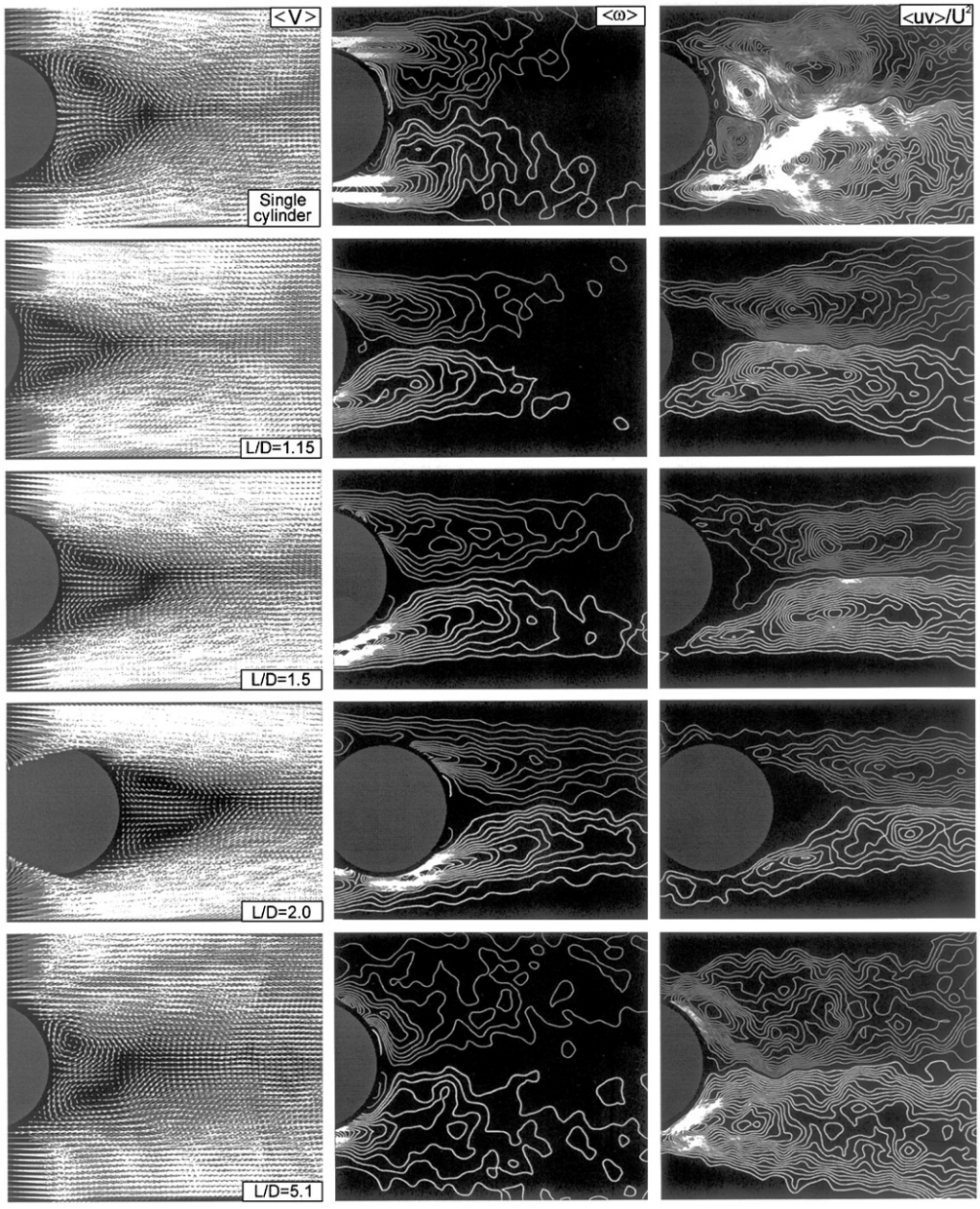

Figure 6. Averaged structure of the near-wake from the downstream cylinder as a function of dimensionless cylinder spacing L/D. Patterns of velocity $\langle V \rangle$, vorticity $\langle \omega \rangle$ and Reynolds stress $\langle uv \rangle / U^2$ are illustrated. All averages correspond to a time average, i.e., no phase reference was employed. For vorticity patterns, minimum $\langle \omega_{\min} \rangle$ and incremental $\langle \Delta\omega \rangle$ are both $2\,s^{-1}$. For constant Reynolds stress normalized by the free-stream velocity, $\langle uv \rangle / U^2$, minimum and incremental levels are both 0·005.

spacing $L/D = 1{\cdot}15$, $1{\cdot}5$, $2{\cdot}0$ and $5{\cdot}1$. The left column of images shows a phase-averaged representation of the velocity field $\langle V \rangle_p$ for each case. The phase reference corresponds to the instant at which formation of the large-scale vortex is completed from the upper surface of the cylinder. Four of these images were averaged in order to obtain the phase-averaged representation $\langle V \rangle_p$. The middle column shows a representative pattern of instantaneous velocity V at the same phase. Finally, the corresponding patterns of instantaneous vorticity are given in the right column. Relative to the case of the single cylinder, patterns corresponding to cylinder spacing $L/D = 1{\cdot}15$, $1{\cdot}5$ and $2{\cdot}0$ show a substantially narrower wake and formation of elongated vortices from the surface of the cylinder. At $L/D = 2{\cdot}0$, the patterns of velocity and vorticity along the upper and lower sides of the wake tend to become symmetrical. In contrast, at $L/D = 5{\cdot}1$, the near-wake pattern is markedly asymmetrical, and the initial, large-scale vortex is formed very close to the base of the cylinder.

These features are further evident in the patterns of velocity and vorticity shown in Fig. 5. The left column again shows, as a reference, the same patterns of phase-averaged velocity vectors $\langle V \rangle_p$ as in Fig. 4. The images of the middle and right columns compare the patterns of phase-averaged vorticity $\langle \omega \rangle_p$ at values of phase separated by π. The near-wake patterns therefore tend to be mirror images of each other.

The consequence of these patterns of vortex formation on the time-averaged structure of the near-wake is shown in Fig. 6. The patterns of averaged velocity $\langle V \rangle$ exhibited in the left column show a narrowing of the near-wake for $L/D = 1{\cdot}15$, $1{\cdot}5$ and $2{\cdot}0$, relative to the case of the single cylinder. At $L/D = 5{\cdot}1$, this wake width is ill-defined, and exhibits a degree of asymmetry.

Patterns of time-averaged vorticity $\langle \omega \rangle$ given in the middle column of Fig. 6 show further features of the narrowed near-wake at $L/D = 1{\cdot}15-2{\cdot}0$. It is evident that both the positive and negative shear layers from the cylinder are deflected inwards toward the plane of symmetry of the near-wake, relative to the case of a single cylinder, where they tend to remain essentially parallel to the plane of symmetry, then degenerate to low levels of vorticity in the central portion of the wake. For the case $L/D = 5{\cdot}1$, for which Kármán vortex formation occurs upstream of the cylinder, the region of high vorticity of each of the shear layers tends to remain close to the surface of the cylinder in the base region. Considering the overall pattern of averaged vorticity $\langle \omega \rangle$ at $L/D = 5{\cdot}1$, however, it degenerates to relatively low levels immediately downstream of the base region and, furthermore, the overall patterns of low-level vorticity $\langle \omega \rangle$ appear to be slightly deflected away from the plane of symmetry.

The values of time-averaged Reynolds stress $\langle uv \rangle / U^2$ are represented in the right column of Fig. 6. For the case of the single cylinder, the separated shear layers from the cylinder show a very high level of Reynolds stress at a distance of approximately $0{\cdot}75D$ downstream of the base of the cylinder. This Reynolds stress has a peak value $\langle uv \rangle / U^2 = 0{\cdot}23$, in which U is the freestream velocity. Embedded within these layers of high Reynolds stress are two concentrated regions of $\langle uv \rangle$, each of which is located adjacent to the base of the cylinder, and has an opposite sign relative to the concentrations in each of the respective separated layers from the cylinder. In these concentrations, the peak value of $\langle uv \rangle / U^2 = 0{\cdot}08$. Such concentrations are apparently associated with the relatively strong regions of recirculation near the base of the cylinder, which are evident in the corresponding pattern of averaged velocity $\langle V \rangle$. The pattern of Reynolds stress distributions is very similar to that calculated by Mittal & Balachandar (1995) at a much lower value of Reynolds number. Their peak values of normalized Reynolds stress are $\langle uv \rangle / U^2 = 0{\cdot}19$ in the shear layer and $0{\cdot}11$ in the region immediately adjacent to the base of the cylinder.

The patterns of Reynolds stress for the two-cylinder system and, in particular, for $L/D = 1{\cdot}15$, $1{\cdot}5$ and $2{\cdot}0$, are fundamentally different from the pattern for the single cylinder. First of all, their overall form involves layers of $\langle uv \rangle / U^2$ that are closely spaced. Second, the peak values of Reynolds stress in these layers are significantly lower. For the values of $L/D = 1{\cdot}15$, $1{\cdot}5$, $2{\cdot}0$, these peak values are $\langle uv \rangle / U^2 = 0{\cdot}081$, $0{\cdot}078$ and $0{\cdot}047$, respectively. Third, in the base region of the cylinder, very low levels of Reynolds stress occur, in contrast to the case of a single cylinder, which exhibit the two concentrations of $\langle uv \rangle$ in that region. At the extreme case of $L/D = 5{\cdot}1$, which corresponds to the case where vortex formation occurs upstream of the cylinder, the region near the base of the cylinder shows high levels of Reynolds stress, in contrast to the smaller spacing $L/D = 1{\cdot}15-2{\cdot}0$. Moreover, for $L/D = 5{\cdot}1$, the peak value of $\langle uv \rangle / U^2 = 0{\cdot}097$, compared with that at $L/D = 2{\cdot}0$, for which $\langle uv \rangle / U^2 = 0{\cdot}030$.

Fig. 7 shows patterns of averaged streamlines $\langle \psi \rangle$ in the near-wake. For the case of the single cylinder, the pattern of $\langle \psi \rangle$ shows the well-known recirculation vortices. A similar pattern occurs for values of spacing from $L/D = 1{\cdot}15-2{\cdot}0$; however, it is narrower than the pattern for the single cylinder. In fact, this narrowing of the pattern of recirculation vortices is associated with inclined streamlines exterior to this region. They rapidly converge towards the plane of symmetry of the near-wake.

All of these features are related to the variation of the averaged streamwise velocity $\langle u \rangle$ normalized by the incident free-stream velocity U, i.e., $\langle u \rangle / U$ as shown in the right column of Fig. 7. The largest magnitude of negative $\langle u \rangle / U$ occurs for the single cylinder. This relatively large value of reverse flow in the region near the base of the cylinder is associated with the formation of particularly well-defined, large-scale vortices in the near-wake, as shown in the images of Figs. 4 and 5. For all cases of the two-cylinder system, i.e., all values of L/D, this magnitude is substantially reduced by about 40%. Moreover, the region of negative $\langle u \rangle / U$ occurs in the range $0 \leqslant x/D \leqslant 0{\cdot}6$ to $0{\cdot}8$ for all cases, including the single cylinder. This means that the substantial narrowing of the wake occurs with relatively little change in the movement of the zero velocity crossing at the plane of symmetry. This point can be interpreted as a saddle or half-saddle point in the corresponding images of the streamline patterns.

5. CONCLUDING REMARKS

The instantaneous and averaged flow structure past two circular cylinders in tandem has been interpreted relative to the corresponding structure of flow past a single cylinder. A number of distinguishing features have been identified, as summarized in the following.

(i) *Unstable structure of shear layers along the gap between the cylinders*. The gap region between the cylinders is characterized by two unstable shear layers along its outer boundaries. These shear layers exhibit small-scale Kelvin–Helmholtz vortices, which have a structure similar to that shown in the images of Chyu & Rockwell (1996) for the case of a single cylinder. It is well known that the development of these Kelvin–Helmholtz vortices is a function of Reynolds number. One therefore expects that the critical spacing, i.e., the cylinder spacing at which vortices are shed in the gap region, will be a function of Reynolds number. This sensitivity to Reynolds number is indicated in the visualization of Ljungkrona *et al*. (1991). For a large gap spacing ($L/D = 4$), variation of the Reynolds number was varied over the range $3{\cdot}3 \times 10^3 \leqslant \mathrm{Re} \leqslant 12 \times 10^3$, and dramatic changes of the gap and near-wake flow patterns were observed; most remarkably, no vortex formation occurs in the gap at the lowest Re, while pronounced vortices occur in the gap at the largest Re. Further features of the Reynolds number dependence at different values of gap

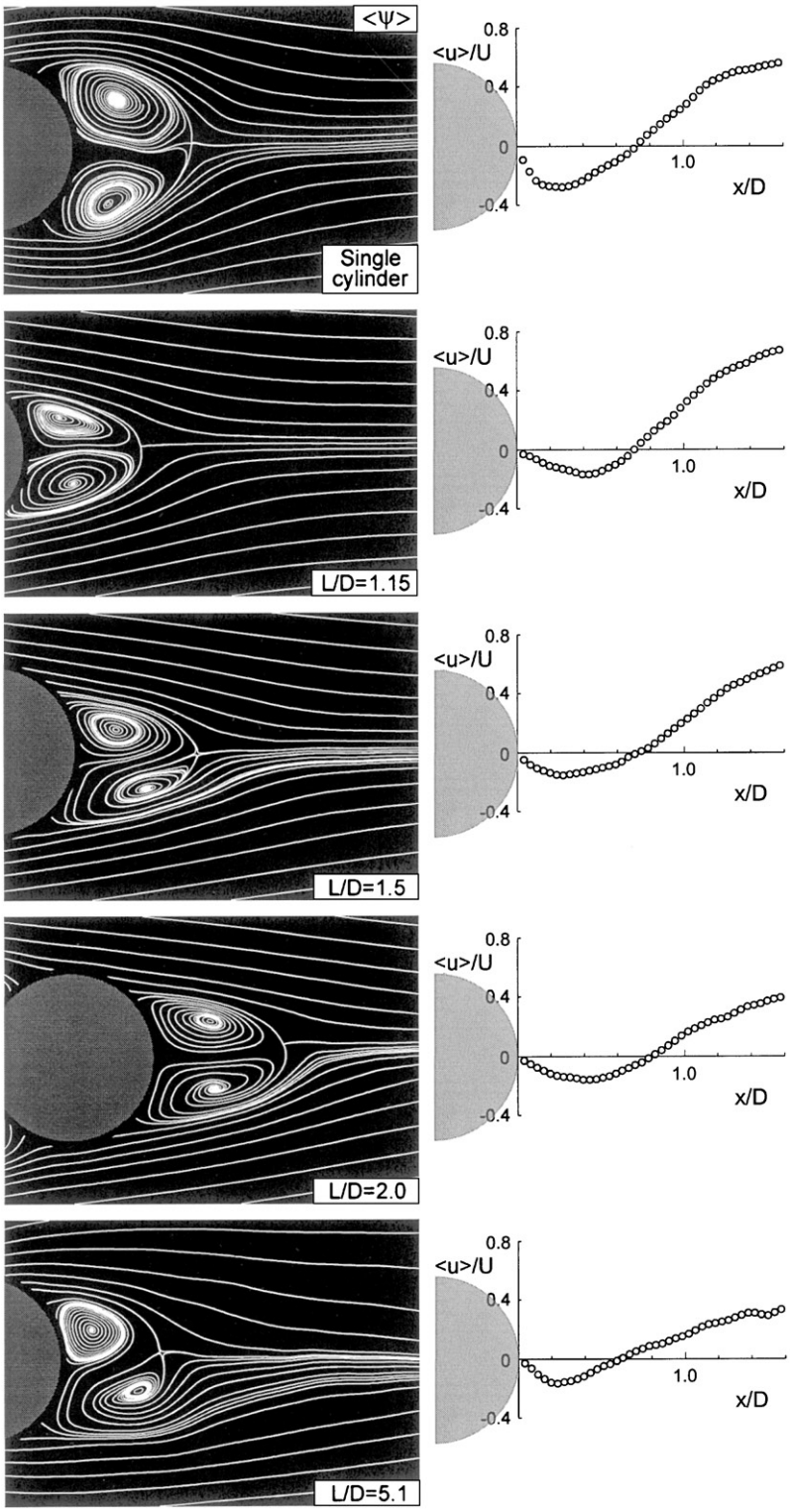

Figure 7. Patterns of averaged streamlines $\langle\psi\rangle$ in the near-wake region of the downstream cylinder. Also illustrated are variations of averaged streamwise velocity $\langle u\rangle/U$ as a function of distance x downstream of the cylinder normalized by the cylinder diameter D.

spacing are shown in the visualization of Ljungkrona & Sundén (1993). Due to the nature of their visualization technique, Kelvin–Helmholtz vortices were not observed in the shear layer, whereas they are visible in the visualization of Ishigai *et al.* (1972) at an equivalent spacing ($L/D = 4$) and Reynolds number ($\mathrm{Re} = 3.4 \times 10^3$) using a different visualization approach. For the case of a single cylinder, significant changes in the pattern of Kelvin–Helmholtz vortices are known to occur when the Reynolds number is varied. Taken together with the present observations of well-defined Kelvin–Helmholtz vortices in the shear layers in the gap region, it is anticipated that enhanced development of the Kelvin–Helmholtz vortices, at higher Reynolds number, will increase both the Reynolds stresses and the entrainment demands of the shear layers, thereby promoting a decrease in the value of the critical gap spacing at higher Reynolds number. Furthermore, at a constant value of Reynolds number, an increase in the level of free-stream turbulence is expected to also enhance the development of Kelvin–Helmholtz vortices. In fact, Ljungkrona *et al.* (1991) found that, as the level of the free-stream turbulence increased, the critical gap spacing decreased.

(ii) *Shear-layer buffeting of downstream cylinder*. In the present configuration, the small-scale Kelvin–Helmholtz vortices formed in the shear layers along the gap eventually buffet the surface of the downstream cylinder. The level of Reynolds stress in these shear layers and the degree to which regions of significant Reynolds stress extend upstream of the impingement cylinder both increase with increasing values of cylinder spacing L/D. These effects are associated with different patterns of Kelvin–Helmholtz vortices in the shear layers. Their scale, as well as the interactions between them, increases with increasing values of dimensionless cylinder spacing L/D. In fact, at sufficiently large L/D, larger clusters of vorticity are evident near the impingement surface of the downstream cylinder. This means that the magnitude of the buffet loading of the downstream cylinder will increase with L/D. In fact, the unsteady pressure measurements of Ljungkrona *et al.* (1991), along the surface of the downstream cylinder, showed elevated values of r.m.s. pressure amplitude as the gap spacing was increased, prior to the critical spacing at which large-scale vortex roll-up occurs in the gap. Furthermore, the r.m.s. pressure distributions of Igarashi (1984) show a pronounced peak at $\theta \cong 60^\circ$, corresponding to the location of impingement of the shear layer. The amplitude of this peak increased with the value of Reynolds number. Similar peaks of the r.m.s. pressure distribution were measured by Ljungkrona & Sundén (1993) at $\theta \cong 75^\circ$ for a lower range of Reynolds number.

A further consequence of this buffet loading is an upstream influence. That is, the unsteadiness in the impingement region will yield velocity and pressure perturbations in the upstream domain of the flow, including the sensitive region of the shear layer at the location of separation from the upstream cylinder. In turn, such perturbations can induce enhanced excitation of the shear layer at this location. These concepts are described by Rockwell (1983) for several classes of impinging shear layers.

(iii) *Recirculation eddies in gap region*. The region between the shear layers along the gap can exhibit patterns of recirculation zones, i.e., eddies. Their strength, as well as their possible asymmetry with respect to the plane of symmetry of the gap, can show substantial intermittency, i.e., variations of instantaneous states. At a sufficiently large gap, a jet-like flow of relatively large magnitude is oriented in the upstream direction along the centerline of the gap region. This effect occurs for a dimensionless cylinder spacing $L/D = 2{\cdot}0$, is mildly evident at $L/D = 1{\cdot}5$, and does not exist at all for $L/D = 1{\cdot}15$.

(iv) *Onset of Kármán vortex shedding and distinctive patterns of Reynolds stress in gap region*. The features of the shear layers bounding the gap, as well as the flow patterns between them, which are defined in items (i) and (iii), are radically altered when the spacing L/D is sufficiently large. In this case, the separating shear layers from the

upstream cylinder feed into the Kármán-like vortices, rather than impinging upon the downstream cylinder. Due to the eventual impingement of the Kármán vortices on the forward face of the downstream cylinder, a remarkably ordered pattern of Reynolds stress $\langle uv \rangle / U^2$ occurs in this region.

(v) *Vortex shedding in near-wake of downstream cylinder*. All of the aforementioned observations have important consequences for the near-wake from the downstream cylinder. For values of cylinder spacing L/D up to $L/D = 2{\cdot}0$, the Kármán-like vortices have a fundamentally different shape and orientation than those formed from a single cylinder. They become elongated with a tendency not to cut the opposing shear layer during the formation process. On the other hand, when the value of L/D is sufficiently large, Kármán shedding occurs in the gap region, and large-scale, Kármán-like vortices are formed very close to the base of the downstream cylinder.

The smoke visualization of Ljungkrona & Sundén (1993) also indicate rapid onset of the Kármán vortex from the downstream cylinder at a large value of gap spacing ($L/D = 4$). The present results indicate that vortical structures incident upon the downstream cylinder are severely distorted as they are swept about the cylinder and, in turn, predispose shedding from the cylinder. This process is accompanied by high values of Reynolds stress on both the upstream and downstream surfaces of the cylinder. Furthermore, all of the foregoing processes result in a Kármán-like vortex street that is wider than the street from a single cylinder.

(vi) *Time-averaged patterns of near-wake of downstream cylinder*. Changes of the time-averaged features of the near-wake from the downstream cylinder are related to the aforementioned changes in Kármán-like shedding. Patterns of averaged vorticity $\langle \omega \rangle$ indicate that, at least up to $L/D = 2{\cdot}0$, the separating layers from the cylinder are remarkably deflected towards the plane of symmetry of the cylinder. That is, the wake appears to narrow significantly. Associated with this process is a decrease in the peak value of Reynolds stress of the near-wake shear layers, relative to the case of a single cylinder. In fact, at $L/D = 2{\cdot}0$, this peak Reynolds stress is approximately a factor of five smaller than the peak value for the case of the single cylinder.

At sufficiently large L/D, such that Kármán shedding occurs in the gap region, the separating shear layers are substantially deflected towards the base of the cylinder. For regions immediately downstream of this initial deflection, the patterns of vorticity are substantially broadened and diverge from the plane of the symmetry of the wake. This alteration of the vorticity field is associated with the highest value of Reynolds stress of the two-cylinder system.

(vii) *Classification of flow regimes*. Igarashi (1981) has provided a classification of possible states of the flow in the gap and near-wake region of the two-cylinder system, as a function of both Reynolds number and gap spacing L/D. It was not the intention of the present investigation to provide quantitative images over a wide range of Reynolds number versus L/D spacing, but certain of the observations herein may elucidate some of the regimes described by Igarashi (1981). He describes a synchronized flow regime, whereby the vortex formation due to rollup of the shear layer in the gap region and the vortex shedding in the near-wake of the downstream cylinder are synchronized with the attachment of the gap shear layer to the other side of the downstream cylinder. Images presented herein suggest a degree of communication between vortex roll-up in the gap region and in the near-wake of the downstream cylinder. For example, in Fig. 2(a), the patterns of velocity corresponding to images (iii) and (v) both show a well-defined swirl pattern in the lower region of the gap and a corresponding swirl pattern in the lower region of the near-wake of the downstream cylinder. Although this mechanism may not be equivalent to that of Igarashi (1981), it does suggest an interrelationship between the gap

and near-wake regions. Another regime, which occurs at larger values of gap L/D, is termed a quasi-stationary vortex regime by Igarashi. Although these types of vortices in the gap region are certainly not due to Kármán-like shedding, the present imaging shows that they exhibit time-dependent states, involving instantaneous asymmetries of the flow pattern in the gap region. These features are evident in the images of Fig. 2(a). Further details of the intricate flow structure in the gap region are summarized at the beginning of Section 3.

ACKNOWLEDGEMENTS

The authors are grateful for the support of the NASA-Langley Research Center under Grant No. NAG-1-1885. Supplemental support was provided by the Air Force Office of Scientific Research, Grant No. F49620-00-1-0009 (533052), the Office of Naval Research, Grants No. N00014-1-0815 (533679) and N00014-98-1-0817 (533699), and the National Science Foundation under Grant No. CTS-9803734 (539442).

REFERENCES

Arie, M., Kiya, M., Moriya, M. & Mori, H. 1983 Pressure fluctuations on the surface of two circular cylinders in tandem arrangement. *ASME Journal of Fluids Engineering* **105,** 161–167.

Chen, S. S. 1984 Guidelines for instability flow velocity of tube arrays in crossflow. *Journal of Sound and Vibration* **93,** 439–455.

Chen, S. S. 1987 *Flow Induced Vibration of Circular Cylinders*. Berlin: Springer-Verlag.

Chen, Y. N. 1985 Flow-induced vibrations of in-line heat exchangers. In Proceedings of ASME Symposium on Flow-Induced Vibrations, **3** (eds. M. P. Païdoussis, J. Chenoweth and J. M. Bernstein), 163-170, New York: ASME.

Chyu, C.-K. & Rockwell, D. 1996 Near-wake structure of an oscillating cylinder: effect of controlled kelvin-helmholtz vortices. *Journal of Fluid Mechanics* **322,** 21–49.

Farrant, T., Tan, M. & Price, W. G. 2000 A cell boundary element method applied to laminar vortex-shedding from arrays of cylinders in various arrangements. *Journal of Fluids and Structures* **14,** 375-402.

Gaydon, M. & Rockwell, D. 1999 Vortices incident upon an oscillating cylinder: flow structure and loading. *Journal of Fluids and Structures* **13,** 709–722.

Hetz, A. A., Dhaubhadel, M. N. & Telionis, D. P. 1991 Vortex shedding over five in-line cylinders. *Journal of Fluids and Structures* **5,** 243–257.

Hiwada, M., Mabuchi, I. & Yanagihara, H. 1982 Fluid flow and heat transfer around two circular cylinders. *Bulletin of the JSME* **25,** 1737–1745.

Igarashi, T. 1981 Characteristics of the flow around two circular cylinders arranged in tandem (part 1). *Bulletin of JSME* **24,** 323–331.

Igarashi, T. 1984 Characteristics of the flow around two circular cylinders arranged in tandem (page 2). *Bulletin of JSME* **27,** 2380–2387.

Ishigai, S., Nishikawa, E., Nishimura, K. & Cho, K. 1972 Experimental study on structure of gas flow in tube banks with tube axes normal to flow (Part 1, Karman vortex flow from two tubes at various spacings). *Bulletin of the JSME* **15,** 949–956.

King, R. & Johns, J. 1976 Wake interaction experiments with two flexible circular cylinders in flowing water. *Journal of Sound and Vibration* **45,** 259–283.

Knisely, C. W. & Kawagoe, M. 1990 Force–displacement measurements on closely spaced tandem cylinders. *Journal of Wind Engineering and Industrial Aerodynamics* **33**, 81-90.

Knisely, C. W. & Nakagawa, H. 1988 Delay time model for tandem cylinder vibration. *Journal of Hydroscience and Hydraulic Engineering* **6,** 1–15.

Knisely, C. W., Gaydon, M. A. & Anderson, R. W. 1995 Effect of upstream separation geometry on the vibrations of the downstream cylinder of a staggered cylinder pair. In Flow-Induced Vibration (ed. P. W. Bearman), Rotterdam: Balkema Press.

LEE, T. & PANAGAKOS, A. 1997 Investigation of boundary layer behavior on single and tandem cylinders. *Fluid–Structure Interaction, Aeroelasticity, Flow-Induced Vibration and Noise*. Vol. **1**, AD-Vol. 53-1, pp. 103–112.

LJUNGKRONA, L. & SUNDÉN, B. 1993 Flow visualization and surface pressure measurement on two tubes in an inline arrangement. *Experimental Thermal and Fluid Science* **6,** 15–27.

LJUNGKRONA, L., NORBERG, C. H. & SUNDÉN, B. 1991 Free-stream turbulence and tube spacing effects on surface pressure fluctuations for two tubes in an in-line arrangement. *Journal of Fluids and Structures* **5,** 701–727.

MAHIR, N. & ROCKWELL, D. 1996 Vortex formation from a forced system of two cylinders. Part I: Tandem arrangement. *Journal of Fluids and Structures* **10,** 473–489.

MITTAL, R. & BALACHANDAR, S. 1995 Effect of three-dimensionality on the lift and drag of the nominally two-dimensional cylinders. *Physics of Fluids* **7,** 1841–1865.

MITTAL, S., KUMAR, V. & RAGHUVANSHI, A. 1997 Unsteady incompressible flows past two cylinders in tandem and staggered arrangements. *International Journal for Numerical Methods in Fluids* **25,** 1315–1344.

PAÏDOUSSIS, M. P. 1982 A review of flow-induced vibrations in reactors and reactor components. *Nuclear Engineering and Design* **74,** 31–60.

PAÏDOUSSIS, M. P. & PRICE, S. J. 1988 The mechanisms underlying flow-induced instabilities of cylinder arrays in crossflow. *Journal of Fluid Mechanics* **187,** 45–59.

PRICE, S. J. & SERDULA, C. D. 1995 Flow visualization of vortex shedding around multi-tube marine risers in a steady current. *In Flow-Induced Vibration* (ed. P. W. Bearman), pp. 483–493. Rotterdam: A. A. Balkema Press.

ROCKWELL, D. 1983 Oscillations of impinging shear layers. *AIAA Journal* **21,** 645–664.

SLAOUTI, A. & STANSBY, P. K. 1992 Flow around two circular cylinders by the random-vortex method. *Journal of Fluids and Structures* **6,** 641–670.

STANSBY, P. K., SMITH, P. A. & PENOYRE, R. 1987 Flow around multiple cylinders by the vortex method. In *Proceedings International Conference on Flow Induced Vibration*, pp. 41–50. Bowness-on-Windermere, England, Cranfield, UK: BHRS.

SUMNER, D., PRICE, S. J. & PAÏDOUSSIS, M. P. 2000 Flow-pattern identification for two staggered circular cylinders in cross-flow. *Journal of Fluid Mechanics* **411,** 263–303.

WEAVER, D. S. & FITZPATRICK, J. A. 1988 A review of cross-flow induced vibrations in heat exchanger tube arrays. *Journal of Fluids and Structures* **2**, 73–93.

WU, J., WELCH, L. W., WELSH, M. C., SHERIDAN, J. & WALKER, G. J. 1994 Spanwise wake structures of a circular cylinder and two circular cylinders in tandem. *Experimental Thermal and Fluid Science* **9,** 299–308.

ZDRAVKOVICH, M. M. 1977 Review of flow interference between two circular cylinders in various arrangements. *ASME Journal of Fluids Engineering* **99,** 618–633.

ZDRAVKOVICH, M. M. 1982 Flow induced oscillations of two interfering circular cylinders. In *Proceedings International Conference on Flow Induced Vibration*, pp. 141–154. Bowness-on-Windermere, England, Cranfield, UK: BHRS.

ZDRAVKOVICH, M. M. 1985 Flow induced oscillations of two interfering circular cylinders. *Journal of Sound and Vibration* **101,** 511–521.

ZDRAVKOVICH, M. M. 1987 The effects of interference between circular cylinders in cross flow. *Journal of Fluids and Structures* **1,** 239–261.

ZDRAVKOVICH, M. M. & PRIDDEN, D. L. 1977 Interference between two circular cylinders: series of unexpected discontinuities. *Journal of Wind Engineering and Industrial Aerodynamics* **2,** 255–270.

ZIADA, S. & OENGÖREN, A. 1993 Vortex shedding in an in-line tube bundle with large tube spacings. *Journal of Fluids and Structures* **7,** 661–687.